

## **Nonstationary filters, pseudodifferential operators, and their inverses**

Gary F. Margrave and Robert J. Ferguson

### **ABSTRACT**

An inversion scheme for nonstationary filters is presented and explored. Nonstationary filters can be inverted provided that the nonstationary transfer function is known and invertible. The two fundamental nonstationary filter types, convolutional and combinational, play a complementary role in the inversion process in that the inverse of nonstationary convolution is nonstationary combination with the inverted transfer function, and vice-versa. These concepts lead to simple expressions for forward and inverse Q filters, forward and inverse wavefield extrapolators, and for any other circumstance where the nonstationary filter form is known.

Inverse Q filtering with nonstationary combination is very precise and provides a simple analytic formalism for such filters. When done with nonstationary convolution, the result is much less acceptable. This assumes the forward Q filter was convolutional.

Numerical experiments with two different wavefield extrapolators, NSPS and PSPI, are shown for a variety of velocity models. NSPS is a convolutional nonstationary extrapolator while PSPI uses the combination form. For constant or weak velocity gradients either extrapolator can invert the other. When velocity becomes chaotic (random), NSPS is required to invert PSPI and vice-versa. Inversion results also improve, even for chaotic velocities, when the extrapolation step size is decreased. A series of small extrapolation steps can be inverted much more successfully with another series of small inverse steps than with a single step. As step size decreases, so does the distinction between NSPS and PSPI and either one becomes able to invert the other.

### **INTRODUCTION**

Nonstationary filter theory is mathematically similar to the theory of pseudodifferential operators. The latter have been developed over the last 70 years in the applied mathematics community to extend Fourier domain techniques to the solution of partial differential equations with variable coefficients. Though mathematically rich and sophisticated, the theory of pseudodifferential operators has seen only limited use in the applied sciences due, in part, to its complexity. Nonstationary filters offer a simple conceptual model for pseudodifferential operators which suggests their application in many new ways such as time-variant deconvolution and depth migration.

Nonstationary filters come in two distinct forms called convolution and combination (Margrave, 1998). These give identical results in the stationary limit

(corresponding to partial differential equations with constant coefficients) but can differ dramatically when the filter is highly nonstationary (e.g. variable coefficients). The two filter forms can be expressed by a variety of different mathematical formulae; but a simple *windowing analog* (Margrave et al., 1998) provides a fundamental insight. If the nonstationary filter consists of piecewise-constant stationary filter segments, then the convolution form is achieved by: (1) windowing the input data to isolate the portion corresponding to each filter segment, (2) applying the corresponding stationary filter to the windowed data, (3) superimposing the results from all stationary filter segments. This process achieves a true linear superposition of impulse responses. The combination form proceeds in a similar, though complementary, fashion: (1) apply each stationary filter to the input data, (2) window the filtered results to isolate the portion corresponding to each filter segment, (3) superimpose the windowed results. Thus, nonstationary convolution can be visualized as the superposition of windowed-then-filtered data segments while nonstationary combination is the superposition of filtered-then-windowed data segments.

Many interesting geophysics problems can be formulated with these techniques. Examples include wavefield propagation (Fishman and McCoy, 1984, de Hoop, 1995, Margrave and Ferguson, 1997), deconvolution methods (Schoepp and Margrave, 1998), and time-variant filtering (Margrave, 1998). Often the problem formulation is more clear in the case of the forward filter than for the inverse. This is especially true for variable coefficient partial differential equations where the forward problem is easily stated as a pseudodifferential operator. The solution then requires the inverse operator.

This paper begins with a mathematical discussion of an inversion method for nonstationary filters. It is shown that nonstationary combination inverts nonstationary convolution and vice-versa. Since these methods become identical in the stationary limit, it is expected that quasi-stationary problems will be invertible with combination or convolution regardless of the forward filter.

Then an example of a forward and inverse constant-Q filter is shown. The forward Q filter is applied with nonstationary convolution and nonstationary combination is required for the inverse. This result provides simple analytic forms for both forward and inverse Q filters.

Next an extensive example is presented using forward and inverse wavefield extrapolators with a variety of velocity models. Phase-shift extrapolators based on nonstationary convolution (NSPS) or nonstationary combination (PSPI) are used. It is shown that for constant velocity or mild complexity, either NSPS or PSPI accomplishes a good inversion of a forward filter with NSPS. However, for very complex settings, a forward extrapolation with NSPS requires PSPI for inversion and vice-versa.

## THEORY

Nonstationary convolution can be written as a simple “mixed domain” form (Margrave, 1998) by

$$G(f) = \int_{-\infty}^{\infty} \alpha(f,\tau)h(\tau)\exp(-i2\pi f\tau)d\tau. \quad (1)$$

In this expression,  $h$  is an input time series,  $\alpha$  is the nonstationary transfer function prescribing a filter, and  $G$  is the Fourier transform (spectrum) of the filtered time series. The nonstationary transfer function describes the filter by giving the Fourier spectrum of its impulse response as a function of the arrival time of the impulse. An ordinary inverse Fourier transform of  $G$  completes the nonstationary convolution filter. The same filter  $\alpha$  may be applied as a combination filter through

$$\hat{g}(t) = \int_{-\infty}^{\infty} \alpha(f,t)H(f)\exp(i2\pi ft)df \quad (2)$$

where  $H$  is the Fourier transform of  $h$  and  $\hat{g}$  is the combination filtered time series. Only in the stationary limit (where the time dependence of  $\alpha$  vanishes) is the result of equation (2) equal to the inverse Fourier transform of equation (1). The fact that (1) is expressed as a forward Fourier integral and (2) as an inverse, together with the complementary nature of the windowing analogs for both, suggests that a possible inverse to equation (1) might be found through

$$\hat{h}(t) = \int_{-\infty}^{\infty} \alpha(f,t)^{-1}G(f)\exp(i2\pi ft)df \quad (3)$$

(assuming that  $\alpha(f,t) \neq 0$  so that  $\alpha^{-1}(f,t)$  is finite everywhere). Thus, the inversion of nonstationary convolution is postulated to be nonstationary combination with the inverted transfer function. Substitution of equation (1) into (3) and interchanging the order of integration leads to

$$\hat{h}(t) = \int_{-\infty}^{\infty} h(\tau)\Delta(t,\tau)d\tau \quad (4)$$

where

$$\Delta(t,\tau) = \int_{-\infty}^{\infty} \alpha(f,t)\alpha(f,\tau)^{-1}\exp(i2\pi f(t-\tau))df \quad (5)$$

is the resolution kernel of the inversion. The ideal resolution kernel is a delta function

$$\delta(t-\tau) = \int_{-\infty}^{\infty} e^{i2\pi f(t-\tau)}df \quad (6)$$

which is infinite when  $\tau=t$  and zero otherwise.  $\Delta(t,\tau)$  is also infinite when  $\tau=t$  (since  $\alpha(f,t)\alpha(f,\tau)^{-1}$  becomes unity in that case), which suggests a very good inversion, but not necessarily zero otherwise.

## Q FILTER EXAMPLE

As an example, consider the application of forward and inverse Q filters. For this case, an approximate expression for  $\alpha(f,t)$  is (Kjartansson 1980)

$$\alpha(f,t) = w(f) \exp\left(-\pi |f| t/Q + i2\pi f t(1 - v/v(f))\right) \quad (7)$$

where  $w(f)$  is the spectrum of a source waveform, the phase velocity is  $v(f) = v[1 + \ln\{|f/f_0|\}/\{\pi Q\}]$ , and  $f_0$  refers to the frequency at which the reference velocity  $v$  is measured. Given the above form for the nonstationary transfer function, let  $h(t)$  be a reflectivity series in time and  $G(f)$  from equation (1) gives the spectrum of the forward Q filtered result. Equation (3) then prescribes the application of an inverse Q filter.

Figure 1 shows the results of a simulation for a minimum phase source waveform (dominant frequency of 15 Hz) and a Q of 25. The reflectivity is shown in (a), the forward Q filter is applied in (b) and inverse filters have been applied in (c) and (d). In (c), the forward Q filter was applied as a nonstationary convolution using equation (1) while the inverse was a nonstationary combination using equation (3). Trace (d) was created with an inverse using nonstationary convolution via the equation

$$\hat{H}(f) = \int_{-\infty}^{\infty} \alpha(f,t)^{-1} g(\tau) \exp(-i2\pi f \tau) d\tau \quad (8)$$

where  $g(\tau)$  is the inverse Fourier transform of  $G(f)$ . The inverse in (c) is nearly exact while that in (d) is very poor. Aside from a slight ripple, (c) is very close to the original reflectivity (a). The Fourier amplitude spectra of the various traces shown in Figure 1 are in Figure 2. The fidelity of the nonstationary combination inverse of the nonstationary convolution filter is remarkable. The spectra of the original reflectivity (a) and the inversion (c) track identically until just below Nyquist (125 Hz.).

This inversion formalism, though not quite exact leads to a simple analytic form for an inverse Q filter. Such simple analytic approximations are very useful as the basis for robust data processing algorithms.

## WAVEFIELD EXTRAPOLATION EXAMPLES

The extrapolation of scalar wavefields through complex media provides an excellent demonstration of the inversion of nonstationary filters. Margrave and Ferguson (1997) give two explicit forms for nonstationary wavefield extrapolators. These operators extrapolate a monochromatic scalar wavefield,  $\psi(x)$ , a single step in the  $z$  direction given a velocity function which varies arbitrarily with  $x$ . (Fishman and McCoy, 1984 and 1985, address this problem in a more general context.) These extrapolators are nonstationary filters in  $k_x$ , and can thought of as Fourier phase-shift operators which allow the phase- shift to vary rapidly with  $x$ . The  $x$  variation of the phase shift operators is limited only by the extent to which the resulting expression

approximately solves the scalar wave equation. There is no mathematical limit to how rapidly the phase can vary with  $x$ .

### PSPI defined

Phase-shift-plus-interpolation (PSPI) method of Gazdag and Squazerro (1984). PSPI accomplishes an approximate extrapolation through  $v(x)$  using a suitable set of reference velocities  $\{v_j\}$ . For each reference velocity, a constant-velocity phase-shift extrapolation is computed and, by interpolating these into a single result, the extrapolation through  $v(x)$  is simulated. Logically, this process can be taken to the limiting case of an “exhaustive set” of references velocities which means  $\{v_j\}$  contains an entry for each distinct value of  $v(x)$ . In this limit, the details of the interpolation process become irrelevant and the PSPI method converges to (Margrave and Ferguson, 1997)

$$\psi(x,z)_{\text{PSPI}} = \int \varphi(k_x,0)\alpha(k_x,x,z)\exp(-ik_x x)dk_x \quad (9)$$

where  $\varphi(k_x,0)$  is the forward Fourier transform of the input wavefield,  $\psi(x,0)$ ,  $\alpha(k_x,x,z)$  is the nonstationary phase-shift operator, and  $\psi(x,z)$  is the output (extrapolated) wavefield. Specifically

$$\varphi(k_x,0) = \int \psi(x,0)\exp(ik_x x)dx, \quad (10)$$

and  $\alpha(k_x,x,z)$  is the nonstationary wavefield extrapolator given by

$$\alpha(k_x,x,z) = \exp\left(iz\sqrt{\frac{\omega^2}{v(x)^2} - k_x^2}\right). \quad (11)$$

$\psi_{\text{PSPI}}$  is computed as a nonstationary combination filter of  $\psi(x,0)$  ( $\alpha(k_x,x,z)$  is the filter), which equation (9) gives in the mixed form as a generalized inverse Fourier integral. For the remainder of this paper, when the term PSPI is used it will refer to these generalized equations.

### NSPS defined

The second wavefield extrapolation operator is the nonstationary convolution complement to PSPI as given above. Called nonstationary phase-shift (NSPS) it is given by (Margrave and Ferguson, 1997)

$$\varphi(k_x,z)_{\text{NSPS}} = \int \psi(x,0)\alpha(k_x,x,z)\exp(ik_x x)dx \quad (12)$$

where  $\alpha(k_x,x,z)$  is again given by equation (11) and

$$\psi(x,z)_{\text{NSPS}} = \int \varphi(k_x,z)_{\text{NSPS}} \exp(-ik_x x) dk_x. \quad (13)$$

Notice that NSPS applies  $\alpha(k_x,x,z)$  simultaneously with the forward Fourier transform (from  $x$  to  $k_x$ ). In contrast, PSPI applies the same nonstationary filter with the inverse Fourier transform (from  $k_x$  to  $x$ ).

### The windowing analog for PSPI and NSPS

The windowing analog results in very simple expressions for the PSPI and NSPS extrapolators. The derivation is found in Margrave and Ferguson (1997) and begins by assuming that  $v(x)$  is piecewise constant with a countable number of segments. If  $v_j$  denotes the  $j^{\text{th}}$  constant velocity, then define the window set  $\{\Omega_j\}$  such that  $\Omega_j(x)=1$  if  $v(x)=v_j$  and is zero otherwise. Then, it results that  $\psi_{\text{PSPI}}$  may be expressed symbolically as

$$\psi(x,z)_{\text{PSPI}} = \sum_j \left\{ \Omega_j \underset{k_x \Rightarrow x}{\mathbf{IFT}} \left[ \alpha_j \underset{x' \Rightarrow k_x}{\mathbf{FT}} \left( \psi(x',0) \right) \right] \right\} \quad (14)$$

where  $\alpha_j$  is the wavefield extrapolator for constant velocity  $v_j$ . Similarly, NSPS becomes

$$\psi(x,z)_{\text{NSPS}} = \underset{k_x \Rightarrow x}{\mathbf{IFT}} \left\{ \sum_j \left[ \alpha_j \underset{x' \Rightarrow k_x}{\mathbf{FT}} \left( \Omega_j \psi(x',0) \right) \right] \right\}. \quad (15)$$

The only difference between expressions (14) and (15) is the point in the process at which the windows are applied. In PSPI the windows are applied after extrapolation while in NSPS they are applied before. Figures 3 and 4 illustrate these processes for the case of upward wavefield extrapolation (i.e. wavefield modeling).

### Inverse propagator and models defined

The inverse theory presented here suggests that  $\psi_{\text{PSPI}}$  can be inverted, to recover  $\psi(x,0)$ , using the NSPS algorithm and an extrapolator of  $\alpha^{-1}$ . Similarly, it also leads to the expectation that  $\psi_{\text{NSPS}}$  can be inverted using the PSPI algorithm. However, there are other possibilities as well. In the limit of constant velocity, both extrapolation methods approach ordinary phase-shift (Gazdag, 1978) which is easily shown to be its own inverse. This leads to the expectation that PSPI or NSPS will also invert themselves when lateral velocity gradients are weak.

The wavefield extrapolator of equation (11) has a well-known bipolar behavior. When  $|\omega/k_x| > v$ ,  $\alpha$  is a complex sinusoid representing propagating body waves. On the other hand, when  $|\omega/k_x| < v$  it becomes a decaying real exponential that is called an evanescent wave. In this context, an evanescent wave propagates in the lateral

direction but decays exponentially with depth. The evanescent portion of the spectrum can theoretically be recovered in an inversion. However, this is numerically unstable so we will restrict our discussion to non-evanescent energy. Thus,  $\alpha^{-1}$  will mean

$$\alpha(k_x, x, z)^{-1} = \begin{cases} \frac{1}{\alpha(k_x, x, z)}, & \left| \frac{\omega}{k_x} \right| \geq v(x) \\ 0, & \text{otherwise} \end{cases}. \quad (16)$$

A consequence of this definition is that the only meaningful distinction between  $\alpha$  and  $\alpha^{-1}$  is the sign of “z” in the exponent of the complex exponential.

A sequence of examples will serve to illustrate these concepts. Figure 5a shows an input wavefield, representing  $\psi(x,0)$ , which is simply a horizontal set of eight impulses. Figure 5b shows three different velocity models that will be examined: a constant velocity of 2000 m/s, a 3000 m/s lens embedded in a 1500 m/s background, and uniformly distributed random velocities lying between 1500m/s and 2500 m/s. The input dataset was sampled at 10 m in x and .004 seconds in t.

### Constant velocity inversion

Figure 6 shows a 50 m upward extrapolation of  $\psi(x,0)$  using ordinary phase-shift for the constant velocity case. The result,  $\psi(x,z)$ , in the time domain is given in figure 6a while figure 6b shows the  $f-k_x$  amplitude spectrum of the same. It is apparent in Figure 6a that each impulse in  $\psi(x,0)$  has been replaced by a diffraction hyperbola. In the Fourier domain this is a set of well-separated lines which have been truncated by the evanescent boundaries of  $|f/k_x|=v$ . (The  $f/k_x$  spectrum of  $\psi(x,0)$  is simply the same set of lines without the evanescent cutoff.)

Figure 7 shows the inversion results calculated with ordinary phase-shift using  $\alpha^{-1}$ . The time domain result (figure 7a) shows that the inversion reconstructs small  $x$ 's (or “butterflies”) at the position of each impulse. The failure to reconstruct a perfect impulse is a direct consequence of the non-inversion of evanescent energy. The Fourier domain result appears identical to figure 6b because the forward and inverse operations in this example are pure phase-shifts and do not affect the amplitude spectrum. This result is the best possible inversion to be shown here and identical results are expected from PSPI and NSPS (assuming constant velocity) used in any combination of forward and inverse extrapolators.

### High velocity lens inversion

Figure 8 shows a 50 m upward extrapolation using NSPS for the case of the high velocity lens of figure 5b. NSPS was chosen as the forward extrapolator because it constructs a superposition of impulse responses (figure 8a) while PSPI does not. (The PSPI result for this case has discontinuities in the wavefield which correspond to the velocity discontinuities.) The Fourier domain picture shows that the spectral lines

defining the impulses have begun to blur. This is because the wavefield extrapolation operation is no longer a simple phase shift when velocity varies laterally. Instead, the nonstationary phase shift actually alters the output amplitude spectrum because it mixes input wavenumbers.

Figure 9 shows the inversion of the wavefield in figure 8 using NSPS, while figure 10 shows a similar inversion but with PSPI. Away from the velocity discontinuities, both inversions have done quite well, while near the discontinuities there are slight artifacts on both inversions. Inspection of the  $f$ - $k_x$  spectra of the inversions gives a slight edge to the PSPI result. Inversion of NSPS by PSPI shows a slight improvement in the resolution of the discrete spectral lines over inversion of NSPS by NSPS. However, even in this rather severe setting, the differences are subtle.

### **Random velocity variation inversion**

A most extreme inversion test is the case of the random velocity model of figure 5b. In figure 11, the result of using NSPS as the forward extrapolator, again for a 50 m step, is shown. The time domain display (figure 11a) is deceptively simple which illustrates a point about NSPS. Nonstationary convolution, which is the basis for NSPS, simply replaces each point of the input by an impulse response whose form is determined by the local conditions at the point of replacement. The eight impulses of the input wavefield (figure 5a) simply sample eight of the many random velocities (figure 5b) and the result is the superposition of eight different diffraction hyperbolae. The Fourier domain expression of this superposition (figure 11b) shows a complete loss of resolution of the spectral lines. Note that the spectrum still shows clearly defined evanescent boundaries.

The two inversions of the wavefield of figure 11 are shown in figure 12 (NSPS<sup>-1</sup>) and figure 13 (PSPI<sup>-1</sup>). The NSPS inversion has not been very successful at all. The output has an energy concentration at the right time (figure 12a) but there is no resolution of individual impulses. The Fourier amplitude spectrum (figure 12b) shows little evidence of the individual spectral lines. In contrast, the PSPI inversion is very good though its character reveals something fundamental about the PSPI algorithm. The eight impulses have been “resolved” into clusters of small points (figure 13a) instead of the expected “x” patterns. The Fourier domain (figure 13b) shows some definition of the spectral lines but there is no evanescent boundary. All of this evanescent energy is an algorithmic artifact. How this can occur when the inverse operator explicitly does not invert the evanescent energy is a property of nonstationary combination filtering. The windowing analog (figure 4) shows that windowing is the final step prior to superimposing the different constant velocity extrapolations. Rapid lateral velocity variation unavoidably results in strong discontinuities in the superimposed wavefields that move energy into the evanescent region. Reference to figure 3 shows that NSPS will always produce a smooth wavefield superposition and no evanescent artifacts.

A further variation on this example is instructive. Figure 14 shows an upward extrapolation through the random velocity model using the PSPI algorithm.

Comparison with figure 11 shows that the PSPI result has produced evanescent artifacts. Interestingly,  $NSPS^{-1}$  is an excellent inverse for this result as shown in figure 15 while the PSPI inverse (figure 16) is poor. Comparison of figures 15 and 13 shows that the actual inversions are similar and leads to the reasonable expectation that an  $f-k$  evanescent filter applied to 13 will lead to a similar result to figure 15.

### Multiple depth steps

When used in a recursive wave-stepping scheme, the differences between NSPS and PSPI become lessened, especially with respect to the suppression of evanescent energy. Though the output of a particular PSPI step can be troubled with evanescent artifacts, if it is input into a subsequent step, it is immediately filtered to reject evanescent energy, as the windowing analog of Figure 3 reveals. Furthermore, though the constant velocity phase shift results are accurate for any size of extrapolation step, the same cannot be said for variable velocity extrapolators. Both NSPS and PSPI use and assumption of locally constant velocity. This means that the cone of scattered energy emitted from a point (NSPS) or pulled into a point (PSPI) is modeled with straight rays depending on a local velocity. Therefore, a series of small steps should be more accurate than one large one.

Consider the random velocity model and taking five 10 m steps instead of one 50 m step. Also, let each 10 m step have a different random velocity field with the same mean and scatter shown in Figure 5b. Figure 17 shows the result of such an upward extrapolation using PSPI. Comparison of this with Figure 14 shows a much improved result with smoother wavefronts and better (though incomplete) suppression of evanescent energy.

The inversions of the result in Figure 17 were also done with five 10 m steps using the identical velocities to the forward extrapolation. Figure 18 shows the NSPS inversion while Figure 19 shows the PSPI result. Both inversions are quite good and are comparable in quality. Figure 19 is an especially dramatic improvement over the single step result shown in Figure 16. NSPS seems to have done a slightly better job, especially in suppression of evanescent energy.

A similar study to that in Figures 17-20 was also conducted using NSPS for the upward extrapolation; but is not shown for space limitations. The results were quite comparable to the PSPI study and definitely better than the single step results in Figures 11-13. It resulted that a multi-step NSPS can be inverted with either a multi-step NSPS or a multi-step PSPI with only slight differences.

## DISCUSSION AND CONCLUSIONS

Nonstationary filters are mathematically similar to pseudodifferential operators. The inversion of these mathematical forms is of interest in the solution of many geophysical problems including deconvolution and migration.

Nonstationary convolution can be inverted almost exactly by a nonstationary combination with the inverse of the mixed-domain transfer function. In the terminology of pseudodifferential operators, an approximate inverse to a given operator is found by applying the algebraic inverse of the *symbol of the operator* with the mathematical form of the adjoint operator. Nonstationary combination is similarly inverted with a nonstationary convolution.

This is a deterministic process that assumes the nonstationary transfer function is known and that it has no zeros. These conditions are at least approximately met in the cases of constant Q filtering and scalar wave extrapolation through laterally variable media. The result is simple expressions for forward and inverse Q filters and forward and inverse wavefield extrapolation filters.

Numerical simulations show that inverse Q filtering by nonstationary combination achieves very high fidelity. The reflectivity spectrum estimate tracked the initial reflectivity spectrum until nearly Nyquist frequency. A convolutional inverse Q filter did not perform well.

Numerical wavefield extrapolations show that NSPS inverts PSPI and vice-versa. Where velocity complexity is low, both processes are good inverses of themselves. In the case of random media, the self-inverses did not perform well over single-step simulations. However; when the simulation is extended to a recursion over several steps, either process becomes an acceptable inverse for either process in the forward mode.

The multistep results suggest that PSPI and NSPS become more and more similar as the extrapolation step size decreases. Indeed, as the step size becomes infinitesimal the two algorithms become equivalent.

## ACKNOWLEDGEMENTS

We thank the Sponsors of the CREWES Project for their generous financial support of our research.

## REFERENCES

- Fishman, L., and McCoy, J.J., 1984, Derivation and application of extended parabolic wave theories. I. The factorized Helmholtz equation: *J. Math. Phys.*, **25**, 285-296.
- Fishman, L., and McCoy, J.J., 1985, A new class of propagation models based on a factorization of the Helmholtz equation: *Geophys. J. R. astr. Soc.*, **80**, 439-461.
- De Hoop, M.V., 1996, Generalization of the Bremmer coupling series: *J. Math. Phys.*, **37**, 3246-3282.
- Gazdag, J., and Squazzero, P., 1984, Migration of seismic data by phase shift plus interpolation: *Geophysics*, **49**, 124-131.
- Margrave, G.F., 1998, Theory of nonstationary linear filtering in the Fourier domain with application to time-variant filtering: *Geophysics*, **63**, 244-259.
- Margrave, G.F. and Ferguson, R.J., Wavefield extrapolation by nonstationary phase shift: submitted to *Geophysics* October 1997, in final review.
- Schoepp, A.R., and Margrave, G.F., 1998, Improving seismic resolution with nonstationary deconvolution: 68<sup>th</sup> Annual SEG meeting, New Orleans, La.

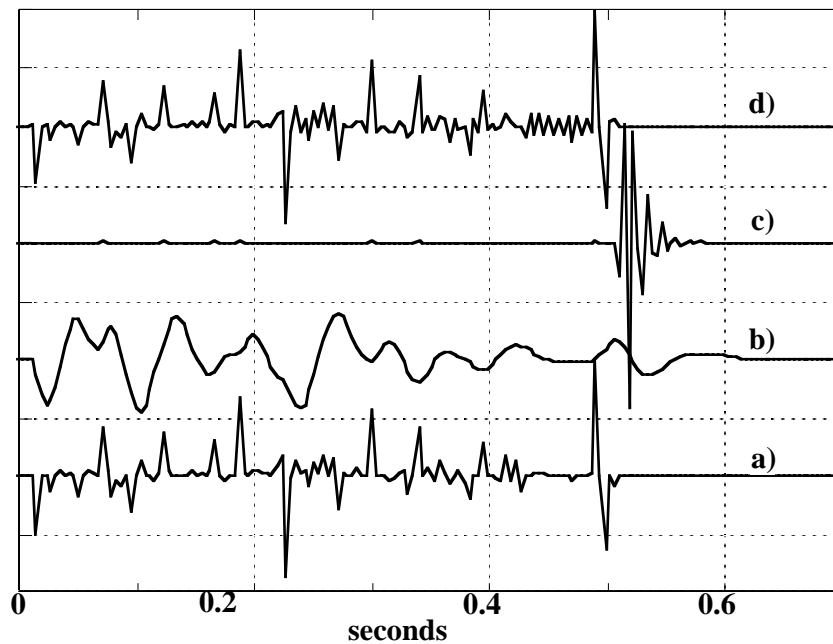


Figure 1. The results of forward and inverse Q filtering are shown in the time domain. The initial reflectivity (a) was filtered with a forward Q filter using nonstationary convolution (b). When nonstationary convolution is used as the inverse process the results are unsatisfactory (c) but when nonstationary combination is used (d) a very good result is obtained.

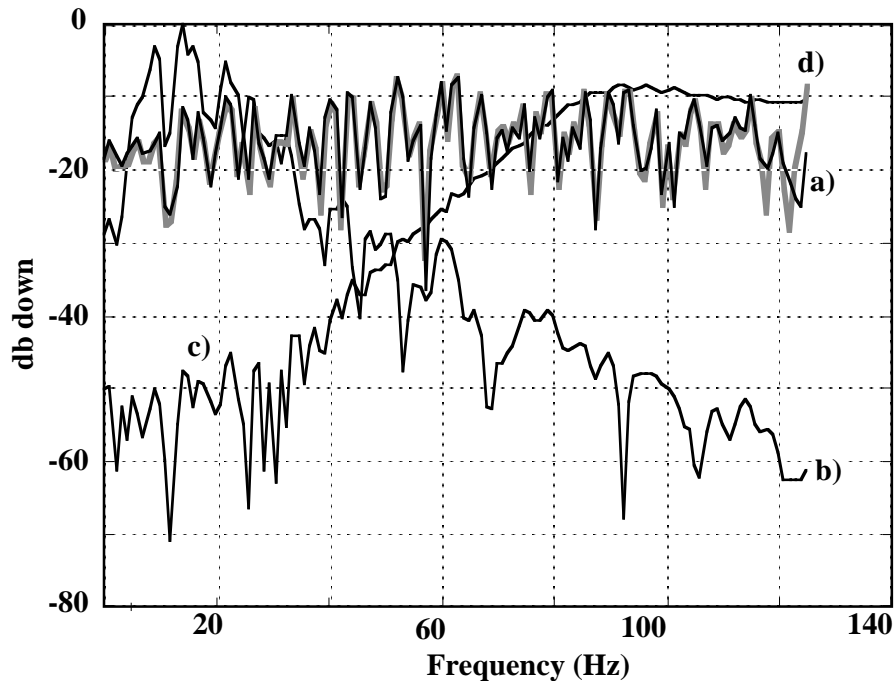


Figure 2. The Fourier amplitude spectra of the traces in Figure 1 are shown. The spectra of the initial reflectivity (a) and the nonstationary combination inverse Q filter (d) are nearly an exact match. The nonstationary convolution inverse Q filter (c) shows a blow-up of the high frequencies. The forward Q filtered spectrum (b) shows very little feature match with (d) which shows that far more that a spectral multiplication was required in the inversion.

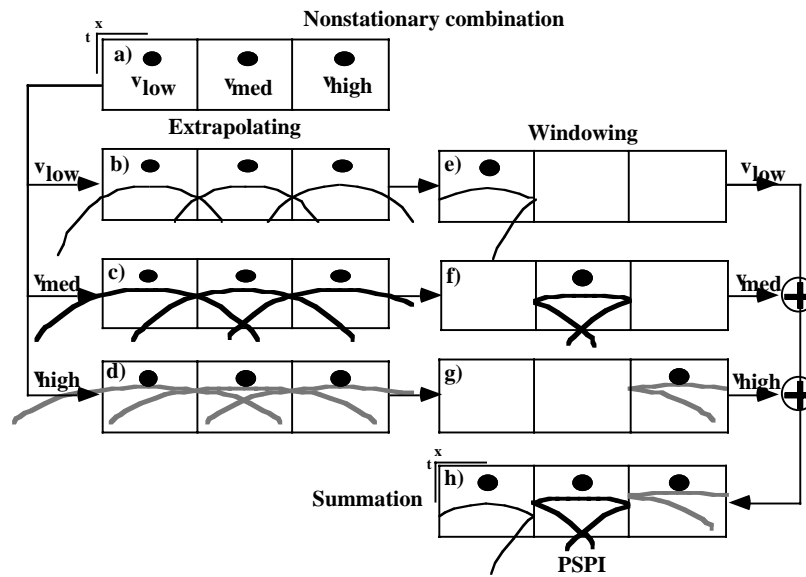


Figure 3. Wavefield extrapolation by nonstationary combination is depicted. The input wavefield (a) consists of 3 impulses in three distinct velocity regions. The first computation step is a complete wavefield extrapolation of the input for each distinct velocity (b), (c), and (d). Next, a boxcar window is applied to each extrapolation which zeros all locations where a particular velocity was not the correct one (e), (f), (g). In the final step, the extrapolated-windowed wavefields are superimposed (h). Note the wavefield discontinuities produced at the velocity boundaries.

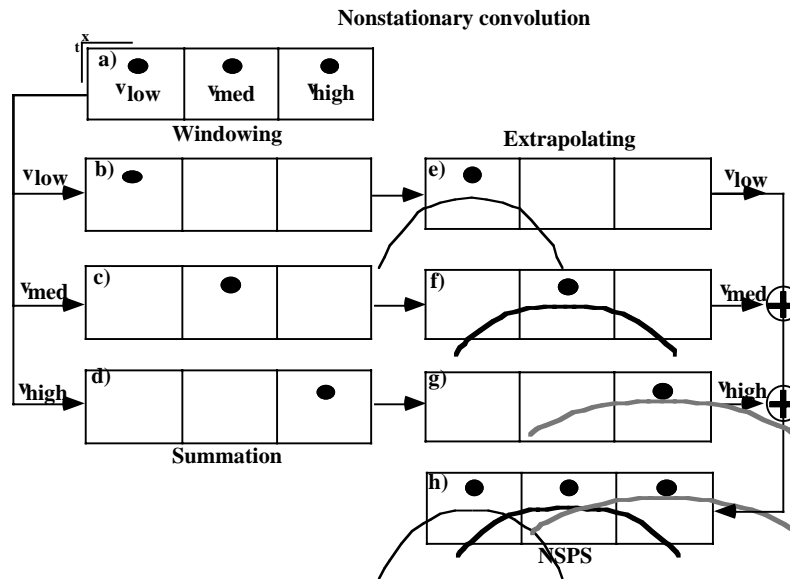


Figure 4. Wavefield extrapolation by nonstationary convolution is depicted. The computation reverses the operations of windowing and extrapolation as described for nonstationary combination (Figure 3). The first computation step windows the input wavefield into three distinct regions which isolated each impulse (b), (c), (d). Next, each windowed wavefield is extrapolated with the appropriate constant velocity (e), (f), (g). In the final step, the extrapolated-windowed wavefields are superimposed (h). The result is a superposition of impulse responses.

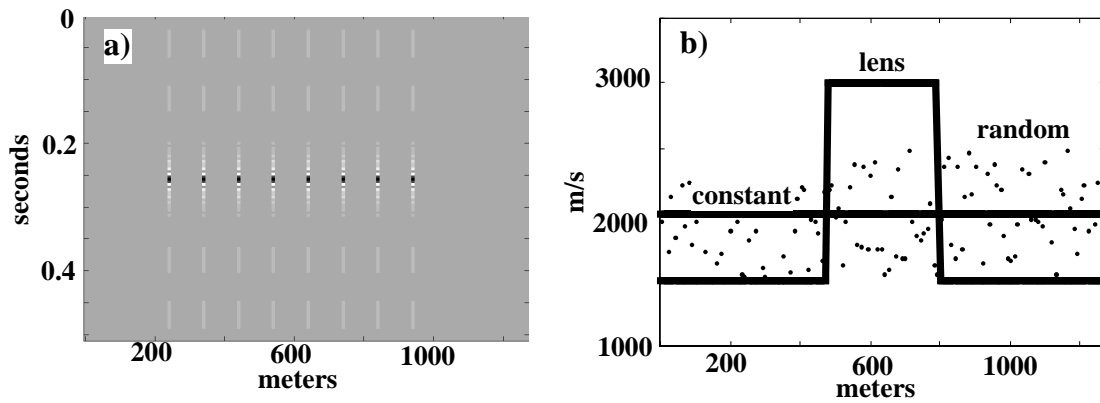


Figure 5. The input wavefield (a) for a series of numerical examples. The spatial sample rate is 10 m and the temporal sample rate is .004 s. Three velocity models are shown in (b): constant, a high velocity lens, and random variation.

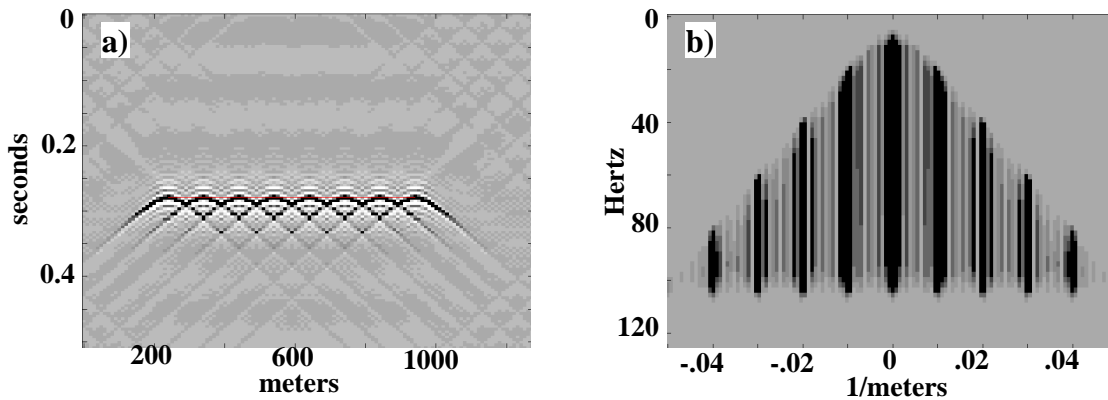


Figure 6. A 50 m upward extrapolation of the dataset of Figure 5a for constant velocity is shown in the space-time domain (a) and the  $f$ - $k_x$  amplitude spectrum (b). Note that each impulse has been replaced by a diffraction hyperbola. The  $f$ - $k_x$  spectrum is characterized by a series of well-separated vertical lines. This is a stationary problem and is presented for comparison with the nonstationary examples.

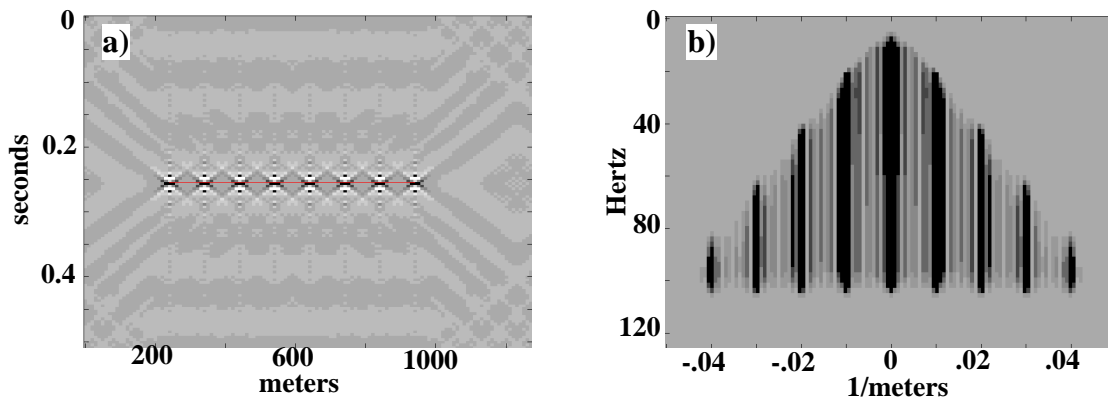


Figure 7. The inverse extrapolation of the wavefield in Figure 6 is shown. The result is the best that can be achieved and images each impulse in an "x" pattern. The  $f$ - $k_x$  spectrum is limited by the evanescent boundaries as evanescent energy was not inverted.

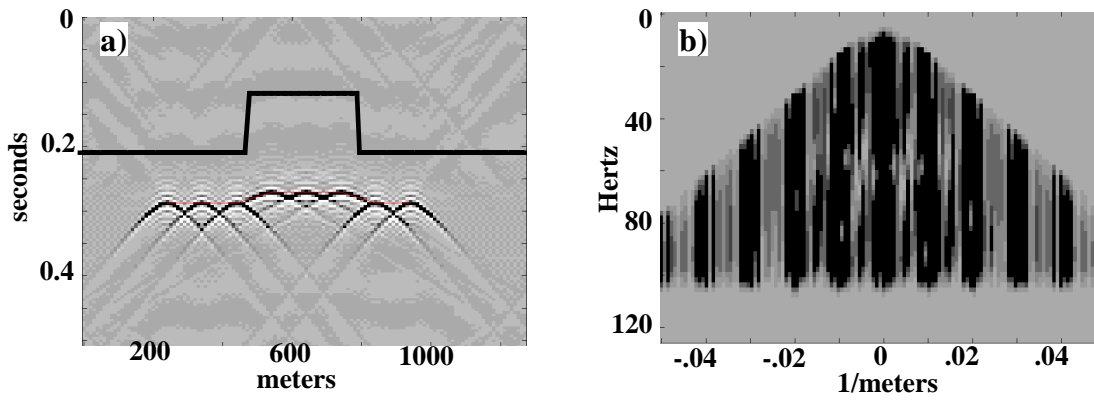


Figure 8. A 50 m upward extrapolation using NSPS of the dataset of Figure 5a is shown in the space-time domain (a) and the Fourier domain (b). The velocity model was the high velocity lens whose position is marked in (a). Note the blurring of the spectral lines in (b).

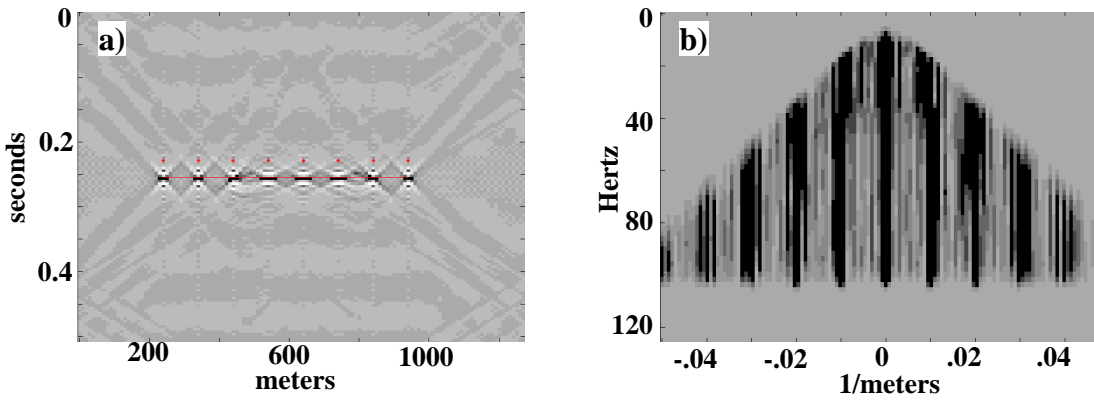


Figure 9. An inverse wavefield extrapolation using NSPS of the dataset of Figure 8 is shown. Good focussing is seen in (a) and the spectral lines (b) have been sharpened. Compare with Figure 10.

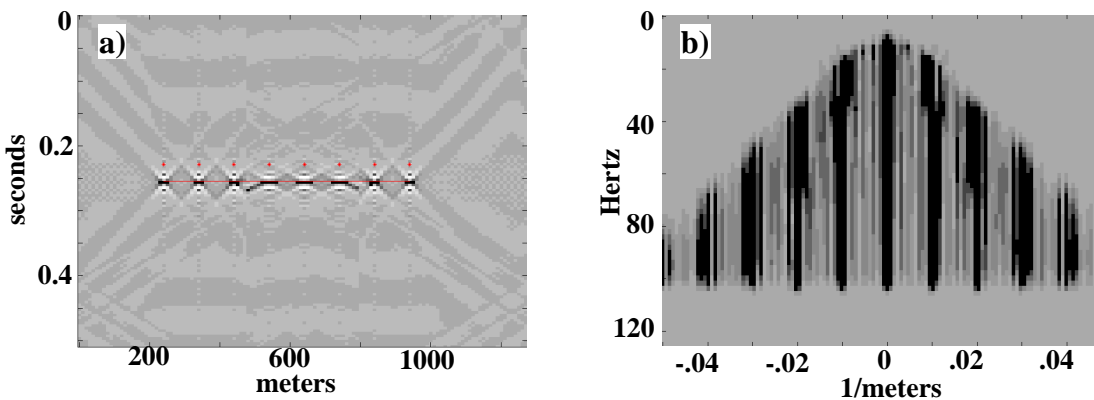


Figure 10. An inverse wavefield extrapolation using PSPI of the dataset of Figure 8 is shown. Good focussing is seen in (a) and the spectral lines (b) have been sharpened.

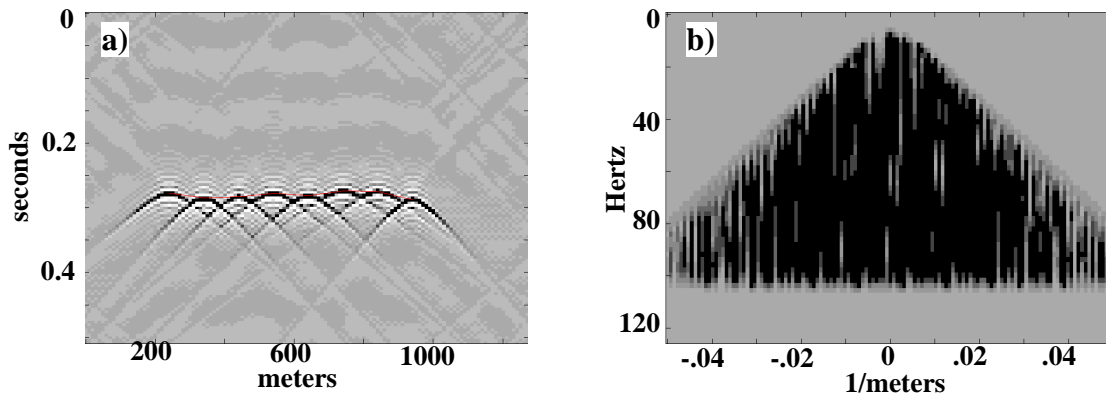


Figure 11. A 50 m upward extrapolation using NSPS of the dataset of Figure 5a is shown in the space-time domain (a) and the Fourier domain (b). The random velocity model was used. Note the complete blurring of the spectral lines in (b).

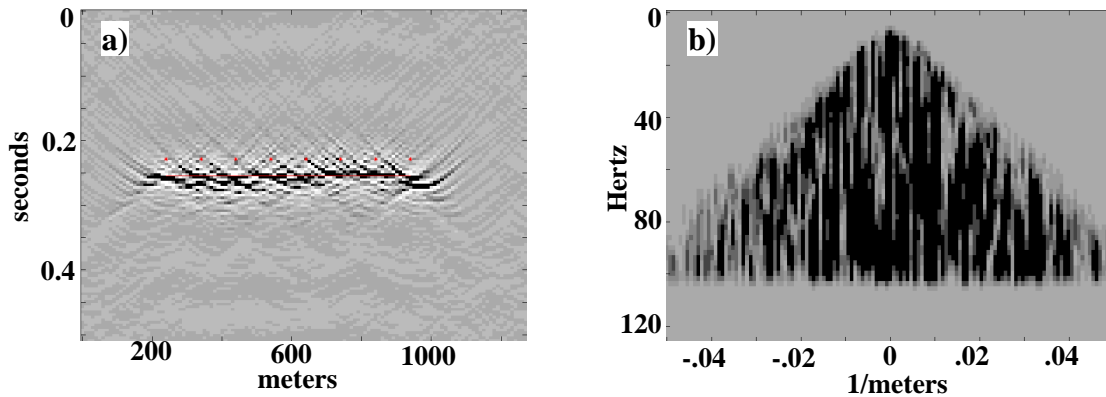


Figure 12. An inverse extrapolation using NSPS of the wavefield of Figure 11. The inversion has failed to resolve the impulses or to define the spectral lines.

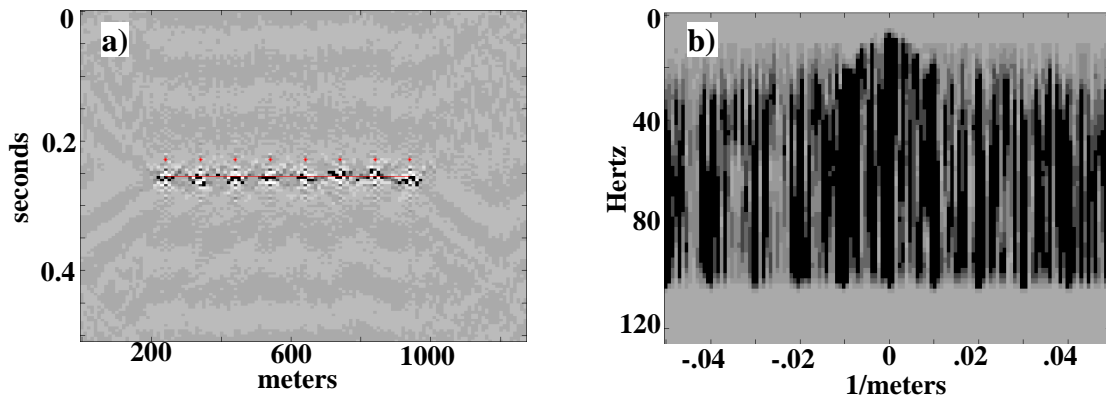


Figure 13. An inverse extrapolation using PSPI of the dataset of Figure 11. The impulses have been resolved as clusters of small points. Though there is some resolution of the spectral lines, there is also a great deal of evanescent energy even though the inversion did not attempt to recover this exponentially damped portion of the wavefield. This was a more successful inversion than that of Figure 12.

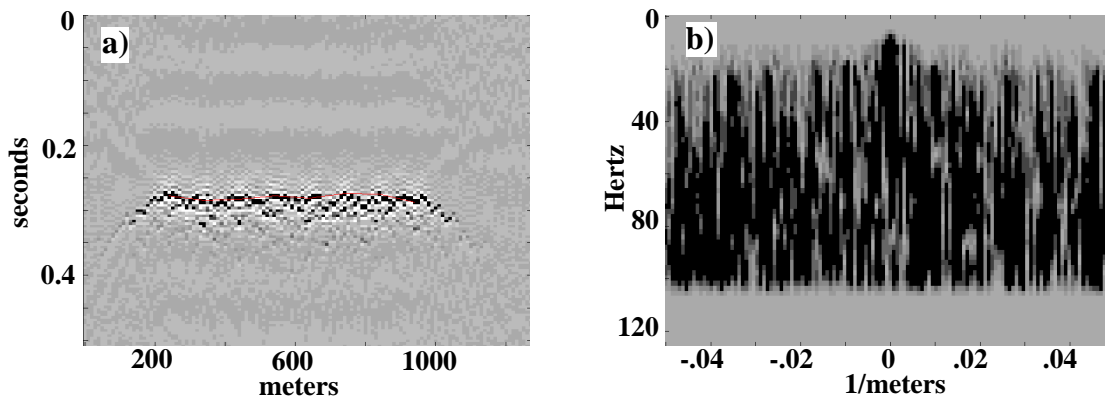


Figure 14. A 50 m upward extrapolation using PSPI of the dataset of Figure 5a and the random velocity model of 5b. Note the chaotic nature of the extrapolation and the creation of evanescent energy even though the extrapolator had a proper exponential decay. Compare with Figure 11.

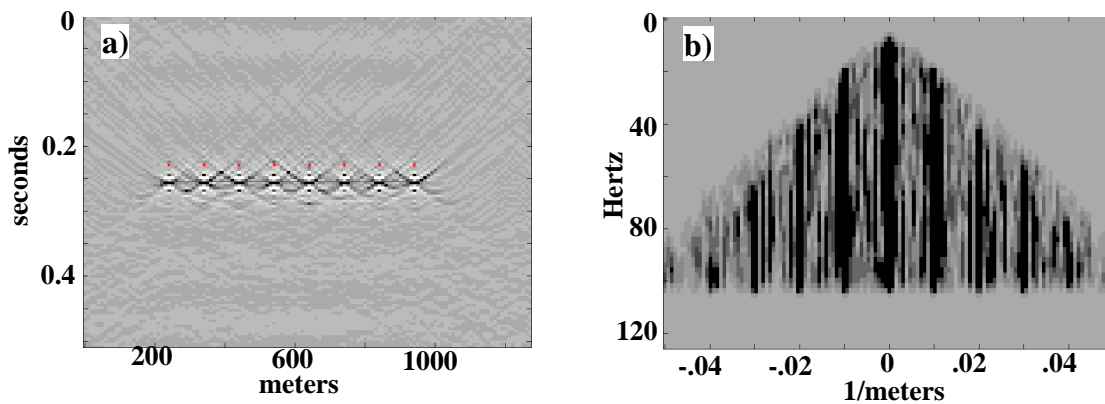


Figure 15. An inverse extrapolation using NSPS of the dataset of Figure 14. The impulses have been resolved into “x” patterns similar to the lens example and the constant velocity example. Note the good separation of the spectral lines and the lack of evanescent artifacts. Compare with Figures 13 and 16.

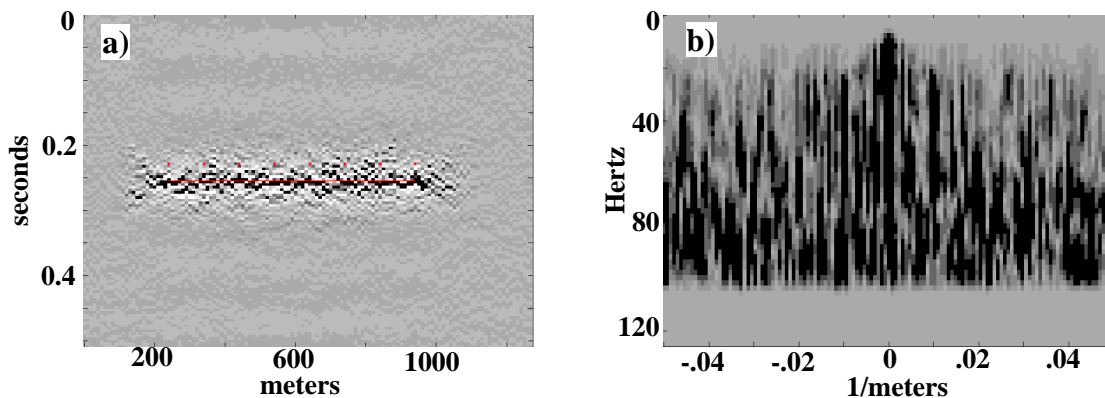


Figure 16. An inverse extrapolation using PSPI of the dataset of Figure 14. The impulses have not been resolved. Compare with Figures 12 and 15.

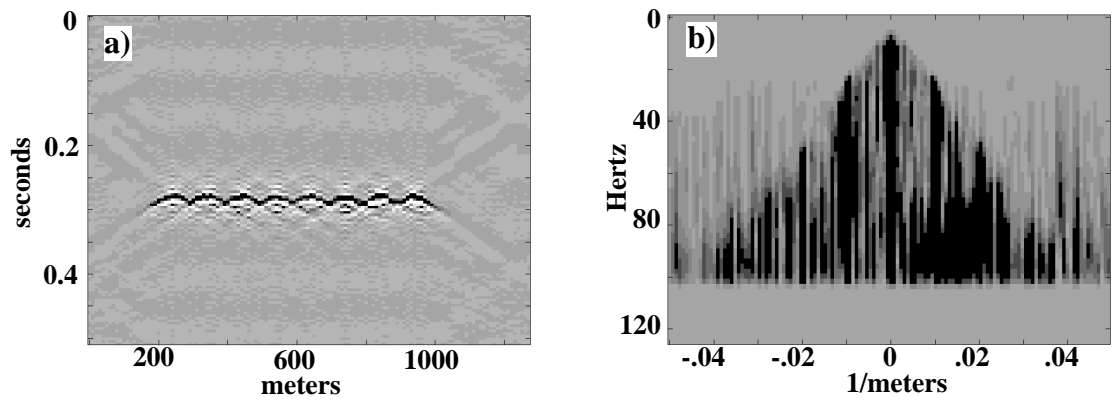


Figure 17. A 50 m upward extrapolation done in five 10 m steps with PSPI. The input dataset is shown in Figure 5a and the velocity field for each 10 m step was a random field with the same mean and variance as that in Figure 5b but with different values for each step. Compare with Figure 14 and note the improvement in the appearance of the wavefield and the better suppression of evanescent energy.

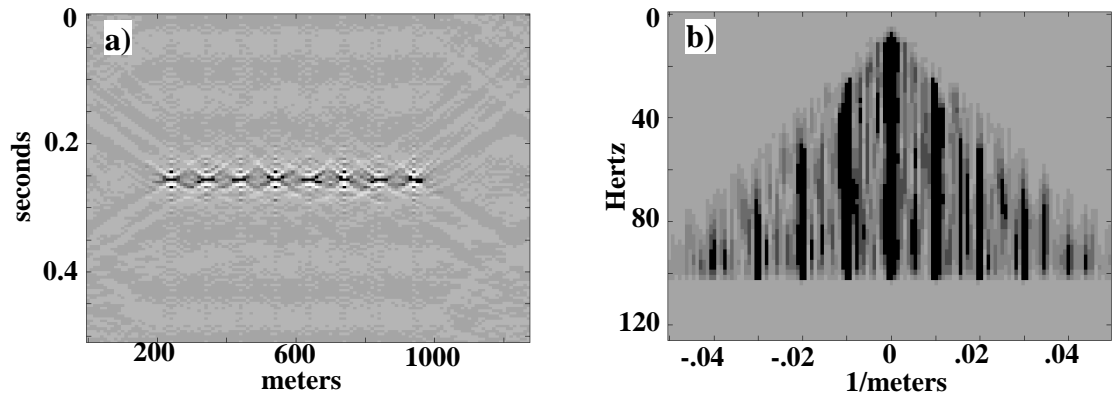


Figure 18. An inverse extrapolation using NSPS of the dataset of Figure 17. The inverse extrapolation was also done in five 10 m steps using the same random velocities as the forward step. In comparison with Figure 15, the inversion is of similar quality.

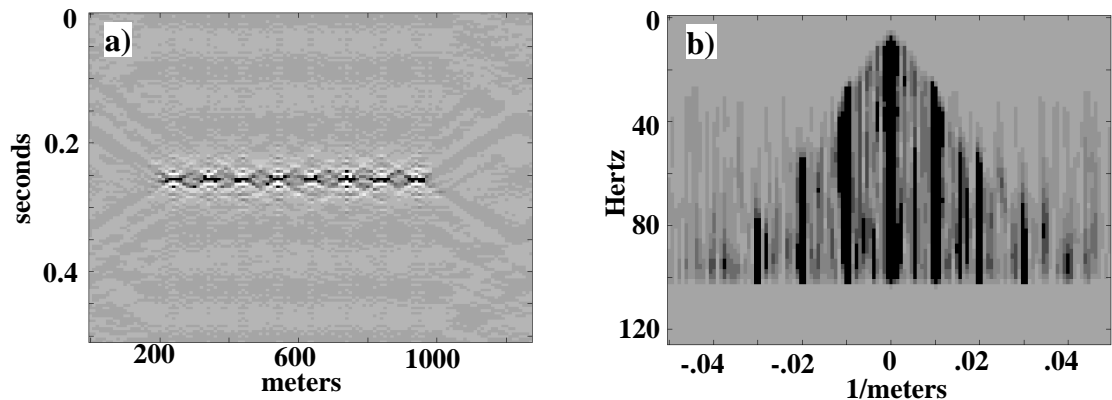


Figure 19. An inverse extrapolation using PSPI of the dataset of Figure 17. The inverse extrapolation was also done in five 10 m steps using the same random velocities as the forward step. This result is much better than that of Figure 16 and is nearly as good as that of Figure 18. Note the improved suppression of evanescent energy relative to Figure 16.